

# The Nondestructive Evaluation of Advanced Ceramics and Ceramic-Matrix Composites

[Jeongguk Kim](#) and [Peter K. Liaw](#)

*In this article, various nondestructive evaluation techniques for advanced ceramics and ceramic-matrix composites are reviewed, and potential nondestructive evaluation methods to control and enhance the manufacturing quality as well as assure the highest level of reliability for monolithic ceramics and ceramic-matrix composites are introduced. These techniques for ceramics and ceramic-matrix composites include ultrasonics, radiography, x-ray computed tomography, and acoustic emission. The principles, experimental procedures, advantages, and limitations of each technique, as well as applications for ceramic materials, are addressed.*

## INTRODUCTION

Ceramic materials, which include monolithic ceramics and ceramic-matrix composites, have been identified as potential candidates for high-temperature structural applications because of their high-temperature strength, light weight, and excellent corrosion and wear resistance.<sup>1</sup> In order to encourage the expanded application of engineering ceramics, the use of appropriate nondestructive evaluation (NDE) approaches is critical to effective process control and the assurance of high-quality products and reliable performance in service.<sup>2-6</sup>

According to the [ASTM](#) Guideline of [Standard Terminology for Nondestructive Examinations](#),<sup>7</sup> NDE or nondestructive testing (NDT) is defined as the development and application of technical methods to examine materials or components in ways that do not impair future usefulness and serviceability in order to detect, locate, measure, and evaluate flaws; to assess integrity, properties, and composition; and to measure geometrical characteristics. Through NDE, the defects and/or flaws in a material can be determined as false, relevant, or nonrelevant indications. This defect information is then evaluated to determine if the component meets specified acceptance criteria. Figure 1 presents a schematic of a typical NDE procedure.<sup>7</sup> Figure 2 shows the linear dimensions of microstructures and defects as well as the resolution capabilities of various NDE techniques.<sup>8</sup>

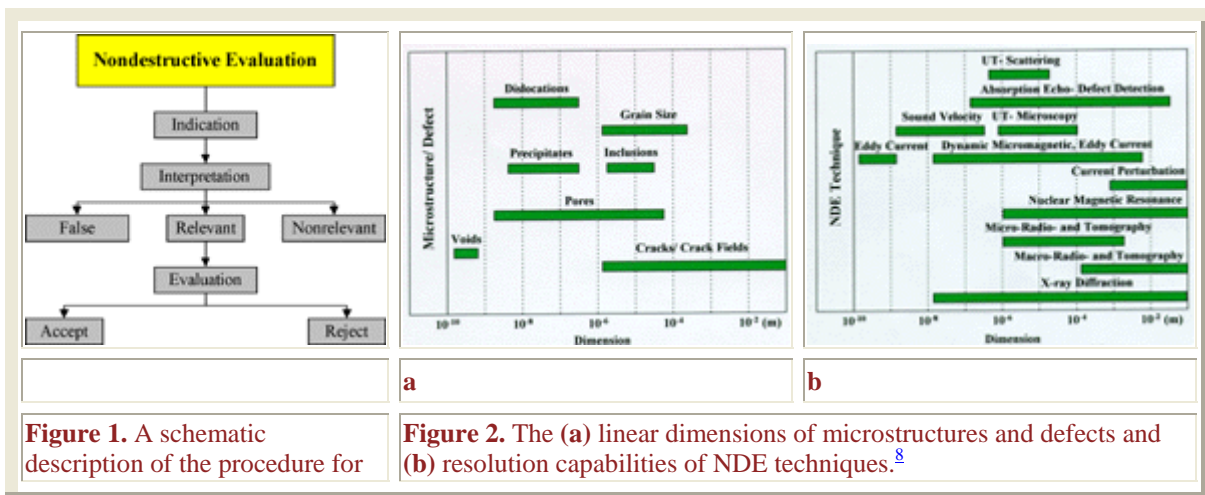


**Figure 1.** A schematic description of the procedure for

**Figure 2.** The (a) linear dimensions of microstructures and defects and (b) resolution capabilities of NDE techniques.<sup>8</sup>

The most important issue in selecting an NDE technique involves the number and types of flaws contained within a material. Generally, monolithic ceramics have some degree of porosity and dislocations; ceramic-matrix composites contain several types of defects, including interlaminar porosity and processing-induced voids.

To consider when and how various NDE techniques can be best applied to the examination of ceramic materials, this paper overviews the following approaches: ultrasonic testing (UT), radiography, x-ray computed tomography (CT), and acoustic emission (AE). Table I provides a comparison of these NDE techniques as applied to the realm of advanced ceramics.

<b>Table I. Key NDE Techniques for Analyzing Advanced Ceramics and Composites</b>				
<b>Characteristics</b>	<b>Ultrasonics</b>	<b>X-ray Computed Tomography</b>	<b>Radiography</b>	<b>Acoustic Emission</b>
Principles	Sonic transmission	X-ray transmission	X-ray, gamma-ray, and neutron transmission of penetrating radiation	Stress wave emission
Variables	Scattering, attenuation, and velocity	Absorption and attenuation coefficients	Absorption and attenuation coefficients	Amplitude, counts, and number of events
Advantages	Suitable for thick materials; relatively quick testing time	Creates cross-sectional view of the entire transmitted thickness	Extensive available database	Real-time monitoring
Limitations	Requires water immersion or acoustic coupling	Expensive; limited specimen size; radiation hazard	Expensive; depth of defect not indicated; radiation hazard	Requires a prehistory of stresses for flaw detection
Detectable Flaws	Voids, delaminations, porosity, and inclusions	Voids, delaminations, porosity, and inclusions	Voids, delaminations, porosity, and inclusions	Delaminations and inclusions

## **ULTRASONIC TESTING**

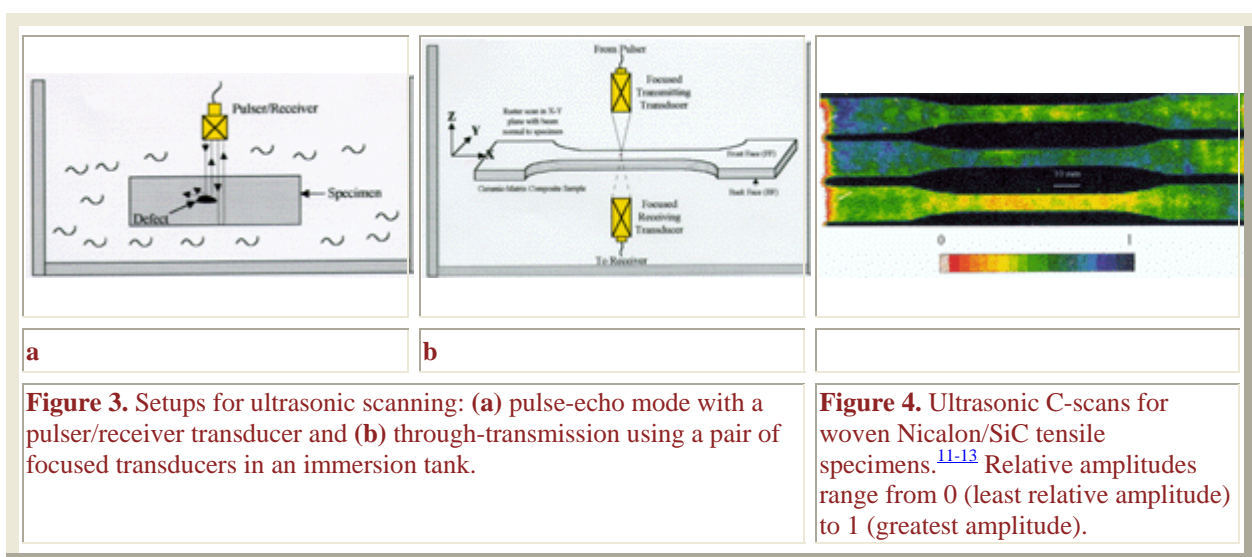
Ultrasonic testing is one of the most widely used NDE techniques for quality-control and service-integrity evaluation because of its relatively inexpensive cost and the convenience of data acquisition. Generally, UT can be used to detect flaws; determine the size, shape, and location of defects; and identify discontinuities of materials. Also, the determination of ultrasonic velocities can be used to measure the modulus of elasticity or Young's modulus of materials.<sup>2-5</sup>

Sound that possesses frequencies so high that it cannot be heard is called ultrasound (the frequency range is typically greater than 20 kHz). In ultrasonic testing, beams of high-frequency sound waves are introduced into materials so as to detect both surface and internal

flaws.<sup>9</sup> The sound waves travel through the material (with some attendant loss of energy) and are deflected at interfaces and/or defects. The deflected beam can be displayed and analyzed to assess the presence of flaws or discontinuities. Most ultrasonic inspections are performed at frequencies between 0.1 MHz and 25 MHz.

A number of ultrasonic evaluation methods—such as A-, B-, and C-scans—have been used to study various types of flaws in ceramic materials.<sup>2-5,10</sup> The UT A-scan presents one-dimensional defect information. In the oscilloscope view, the A-scan signal displays the pulse and amplitude against time. The A-scan display is commonly used to measure material thickness. The UT B-scan displays a parallel set of UT A-scans with two-dimensional data (i.e., the B-scan presents defect distribution through the material's cross section). The B-scan can also be used to inspect rotating tubes and pipes, because it provides a cross-sectional view of defect distribution. The UT C-scan is the most widely used scan mode, as it provides a two-dimensional presentation of defect distribution. A C-scan displays the size and position of flaws in an area parallel to the surface through the raster scan of two axes. A C-scan presentation is a very effective way to investigate flaw distribution, since the presence of the flaw as well as its severity can be readily indicated on a drawing of the part being inspected.

To measure the time of flight or attenuation of the UT signal, the UT scan mode may be employed in either in a through-transmission mode (using both a transmitting transducer and a receiving transducer) or a pulse-echo mode (using a single pulser/receiver transducer). Figure 3 presents a pulse-echo mode setup with a pulser/receiver transducer and the through-transmission ultrasonic (TTU) setup using a pair of focused transducers. The scan is performed in an immersion tank. In Figure 3a, the pulser/receiver transducer is used to generate ultrasonic sound waves and receive the reflected beams. The transducer obtains the traveling sound-wave signals, which are displayed on the oscilloscope with amplitudes against the traveling time. Finally, a computer gathers the amplitudes and forms a scan image. In the TTU mode, the transmitting transducer (pulser) and receiving transducer (receiver) are aligned, and the beam path is kept perpendicular to the test specimen during the scan (Figure 3b). The two transducers are ganged using a yoke arrangement that maintains the alignment of the focused beam.



The reason for selecting the TTU geometry is partly due to the high attenuation of the material and the difficulty in obtaining and interpreting pulse-echo signals. In the TTU

approach, a time gate is applied to encompass the transmitted signal and to record its amplitude during a C-scan. Moreover, the C-scan image was developed by capturing and displaying the transmitted signals in a raster scan along the x-y plane of the test sample (Figure 3b).

The amplitude of the transmitted ultrasonic beam is measured by the receiving transducer, which is also focused and positioned symmetrically with respect to the transmitting transducer. The amplitude of the TTU signal is quite sensitive to the presence of internal defects (e.g., voids and delaminations) and to variations in the internal structure (e.g., undulation of fiber tows in continuous-fiber-reinforced ceramic-matrix composites). Any defects or internal material conditions that attenuate, scatter, or block the transmitting ultrasonic beam will result in a low TTU signal in the C-scan image.

## Experimental Activities

Most UT work has focused on characterizing surface flaws and/or internal defects in ceramic materials.<sup>11-14</sup> Significant work has been accomplished in establishing the modulus measurement and characterization of defect distribution in ceramic materials using UT C-scan amplitudes.<sup>14</sup>

Figure 4 shows UT C-scans of continuous woven Nicalon®-fiber-reinforced SiC ceramic-matrix composites. Nicalon is an amorphous/crystallite fiber, predominantly SiC, with a diameter of approximately 10-15  $\mu\text{m}$  and having a chemical composition of Si-31C<sub>2</sub>-10O<sub>2</sub> (wt.%). Most tensile test specimens were 3 mm thick, 18 mm in width, and 200 mm in length. Specimens with a gage dimension of 10 mm  $\times$  60 mm were machined from the woven composites.

Ultrasonic amplitude measurements were performed using a TTU C-scan mode at a frequency of 15 MHz in an immersion tank (Figure 3b). The transducers had a diameter of 1.27 cm and a focus length of 5.08 cm. Generally, a UT C-scan presentation can be described as consisting of different color scales. In Figure 4, the color scheme is arranged such that blues and greens correspond to high amplitudes of transmitted ultrasonic signals, which are less attenuated by the anomalies and derive from the overall "good" or dense regions in the composites. The reds and yellows represent low amplitudes, which are greatly attenuated by the defects and result from generally "bad" or porous areas. This color scheme is based on the relative amplitude range of transmitted ultrasonic waves. Relative amplitudes range from 0 (least relative amplitude) to 1 (greatest amplitude). Defect distribution is designated as a C-scan in light of the ultrasonic-transmitted amplitudes. In other words, for an area containing a greater amount of defects, more ultrasonic waves will be deflected or scattered by the defects, resulting in the transmitted ultrasonic waves having lower amplitudes.

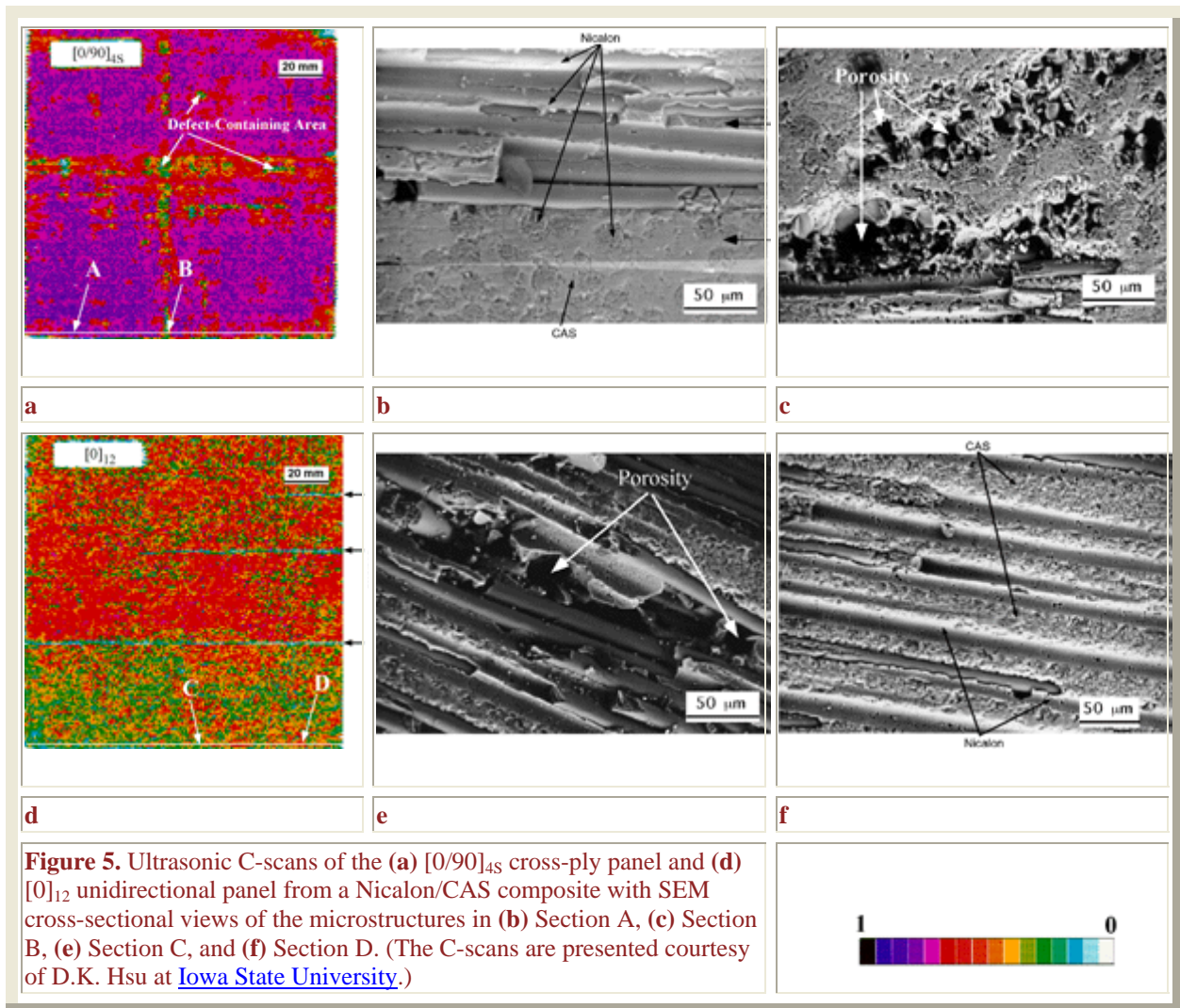


**Figure 5.** Ultrasonic C-scans of the (a)  $[0/90]_{4S}$  cross-ply panel and (d)  $[0]_{12}$  unidirectional panel from a Nicalon/CAS composite with SEM cross-sectional views of the microstructures in (b) Section A, (c) Section B, (e) Section C, and (f) Section D. (The C-scans are presented courtesy of D.K. Hsu at [Iowa State University](http://www.iastate.edu).)

Figure 5 illustrates ultrasonic amplitude measurements derived from continuous-Nicalon-fiber-reinforced calcium aluminosilicate glass ceramic-matrix composites—designated Nicalon/CAS (Corning Glass Works). Two types of materials were prepared: a  $[0/90]_{4S}$  cross-ply composite panel and a  $[0]_{12}$  unidirectional composite panel. All panels had dimensions of 152.4 mm  $\times$  152.4 mm  $\times$  3 mm. For the  $[0/90]_{4S}$  panel, the Nicalon/CAS composite was prepregged into unidirectional plies with a 40% fiber volume and hot-pressed into a  $[0/90]_{4S}$  laminate panel. For the  $[0]_{12}$  unidirectional composite, the Nicalon/CAS composite was supplied in a 12-ply, unidirectionally reinforced ( $[0]_{12}$ ) panel. Fabricated using 500-count fiber tows, this material was produced by hot pressing at about 1,350°C using prepregged unidirectional plies.

In the case of UT for the  $[0/90]_{4S}$  cross-ply panel (Figure 5a), there are variations of ultrasonic amplitude, particularly along a horizontal line and a vertical line through the center of the panel. For the  $[0]_{12}$  unidirectional panel (Figure 5d), the ultrasonic transmitted amplitudes revealed two cracks in addition to the long crack across the width (horizontal line). As a whole, the upper and lower sections of the panel contained more defects than the center section.

Analysis via scanning electron microscopy (SEM) was performed to relate the different amplitude distributions on the panel edges. As shown in Figure 5a, Section A had relatively

greater ultrasonic amplitude values than Section B; hence, the processing-induced porosity was found not in Section A (Figure 5b) but in Section B (Figure 5c). In the case of the [0]<sub>12</sub> unidirectional composite panel, Sections C (lower amplitude values, as shown in Figure 5d) and D (higher amplitude values, again as shown in Figure 5d) were selected for SEM investigation. In Section C (Figure 5e), severe porosity is visible at the fiber-matrix interface; Section D (Figure 5f) reveals good microstructural features. Clearly, the suite of figures that comprise Figure 5 demonstrates that lower ultrasonic amplitudes correspond to the presence of porosity. This occurs because such defects scatter and deflect the UT waves.

Modulus measurements were performed using a dry-coupling ultrasonic technique and specimens machined from woven Nicalon-fabric-reinforced SiC composite disks (Figure 6). Longitudinal moduli along the in-plane (fiber-fabric plane) direction ( $X_1$  or  $X_2$  axis) and through-thickness ( $X_3$ ) direction were determined. Note that along the through-thickness direction, the specimen contained approximately 20 fiber fabric plies. Ultrasonic measurements were performed using longitudinal waves. The longitudinal modulus ( $C$ ) is related to the longitudinal velocity ( $V_L$ ) by

$$C = \rho V_L^2 \quad (1)$$

where  $\rho$  is the density of the composite.

Dry-coupling longitudinal transducers were used because the Nicalon/SiC samples were highly porous and the use of a liquid or gel couplant would change the modulus values, thereby contaminating the samples. The dry contact transducers had a thin elastomer face-sheet and coupled the ultrasonic propagation by pressure, without the aid of a liquid or gel couplant. The transducers had a crystal size of 19.1 mm and a center frequency of 0.5 MHz.

A pulse-echo overlap method was used to measure wave velocity. As depicted in Figure 7, the reference signal was captured by passing ultrasonic longitudinal waves through a sample positioned between a rubber sheet and a fused quartz piece. The received radio-frequency waveforms, with and without a sample in the acoustic path, were matched as closely as possible by shifting one to overlap with the other (hence the name pulse-echo overlap). Since the time shift required for the match is equal to the transmit time of the ultrasonic waves through the sample, the ultrasonic longitudinal velocity is simply the sample thickness divided by the time shift. Both in-plane and through-thickness longitudinal ultrasonic velocities were measured for the composite material and yielded in-plane moduli and through-thickness moduli.

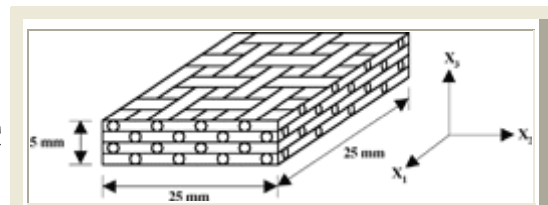


**Figure 6.** An illustration of specimen geometry for the woven Nicalon/SiC composites used in modulus measurements.

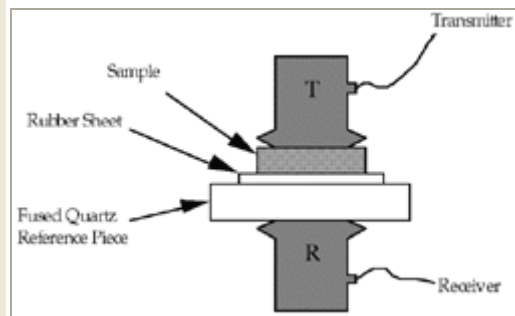


**Figure 7.** Ultrasonic setup for measuring the modulus in Nicalon/SiC composites.<sup>14</sup>

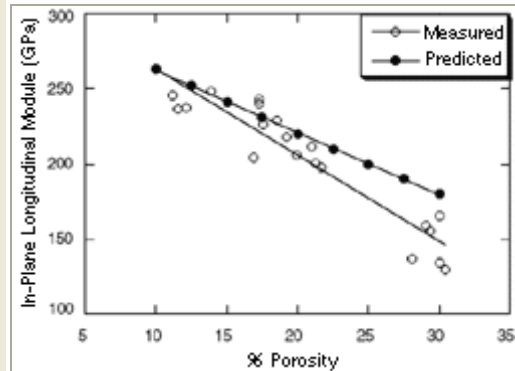


**Figure 8.** A comparison of predicted and measured in-plane longitudinal moduli in Nicalon/SiC composites.<sup>14</sup>

The ultrasonic velocities ( $0.8-1.0 \times 10^4$  m/s) were greater in the in-plane direction than in the through-thickness direction ( $0.17-0.73 \times 10^4$  m/s). Consequently, the in-plane longitudinal moduli (130-248 GPa) were greater than the through-thickness longitudinal moduli (6-138 GPa) as is to be expected from the fabric lay-up.<sup>14</sup> Porosity had a greater effect in reducing ultrasonic velocity in the through-thickness direction than in the in-plane direction. These results derive from the greater interlaminar porosity as compared to the porosity at the fiber-tow intersection.<sup>14</sup> Furthermore, increased porosity significantly decreased both in-plane and through-thickness moduli. It should be noted that the ultrasonic measurements yielded comparable in-plane moduli values along the fiber fabric plane shown in Figure 6.

Figure 8 presents the predicted in-plane moduli of Nicalon/SiC composites versus porosity. Clearly, there is reasonably good agreement between the predicted and the measured moduli. Consistent with what was observed experimentally, increased porosity decreased the stiffness. (Greater detail on the moduli calculation can be found in Reference 14).

## RADIOGRAPHY

There are two primary applications of radiography: determining inherent material properties (e.g., composition, particle size, and density) and evaluating manufacturing properties (e.g., existing flaws and complexities). In radiography, radiation is passed through the subject part or material, and a detector senses variations in the intensity of the radiation exiting the sample, thereby enabling a profile of the internal defect distribution.<sup>15</sup> The resulting two-dimensional radiation pattern can be visualized using photographic films or fluorescent screens. Using this technique, a wide range of material thickness levels can be assessed, as can complex shapes that would be difficult to scan using an ultrasonic technique.

In general, radiographic NDE can be classified according to the type of radiation employed: x-ray, gamma, or neutron.

NDE using x-ray or gamma rays includes capturing and processing a shadow photograph. Specifically, the varying amounts of transmitted radiation cause ionization in the emulsion surface of the film, forming a latent image. The radiographic sensitivity of the resulting photograph is limited by the quality of the shadow image, by the scatter of radiation in the test object, by the test environment, and by the nature of the film emulsion.

In neutron radiography, the image is essentially a two-dimensional shadow display representing the intensity distribution of thermal neutrons passing through an object. As compared to x-ray or gamma-ray radiography, the attenuation characteristics of neutron energy are different. Here, the total neutron cross section is the criterion for utilizing neutron radiography, whereas density and atomic number (linear absorption coefficient) are the main parameters in x-ray and gamma-ray radiography. Generally, neutron radiography complements conventional x-ray and gamma-ray radiography as it can detect flaws and material conditions that other methods cannot effectively assess.

Although radiography has numerous advantages, it is not without certain drawbacks. For example, access to opposite sides of the test object is required, and some structures are not amenable to study (e.g., components in radioactive or high-temperature environments). To maximize the likelihood of detection, cracks must be oriented nearly parallel to the beam. Delaminations are almost always undetectable. Finally, the use of radiography is a health risk, and the technique is expensive.

## Experimental Activities

Neutron radiography has been used to detect various types of discontinuities (e.g., voids and bulk-density reduction) and determine the structure and composition of lithium-based ceramics and glasses.<sup>16</sup>

Lewis et al. conducted extensive work with  $\text{Si}_3\text{N}_4$  composites and  $\text{Al/Si/Al}_2\text{O}_3$  composites to contrast the capabilities of neutron and x-ray radiography.<sup>17</sup> They found that neutron radiography is capable of producing good-quality images on a wider range of ceramic composites than x-ray radiography and that it is better suited for examining thicker sections in these materials.

Highly sensitive microfocus x-ray radiography was used to detect and measure micrometer-sized defects in  $\text{ZrO}_2$  pellets.<sup>18</sup> Artificial flat-bottom holes and saw cuts of different depths were made to the pellets to use as calibration standards.

## X-RAY COMPUTED TOMOGRAPHY

X-ray computed tomography provides a cross-sectional view of an object's interior and is well suited to characterizing a material's integrity.<sup>19,20</sup> In essence, CT is an advanced form of x-ray radiography. Conventional radiography provides a two-dimensional presentation of a three-dimensional object as the image plane is approximately normal to the x-ray beam. CT creates a digital representation of a thin slice parallel to the x-ray beam. Typical slice thickness ranges from 0.025 mm to 3 mm, with pixel sizes (picture elements) ranging from 0.025 mm to 1 mm.<sup>19,21,22</sup>

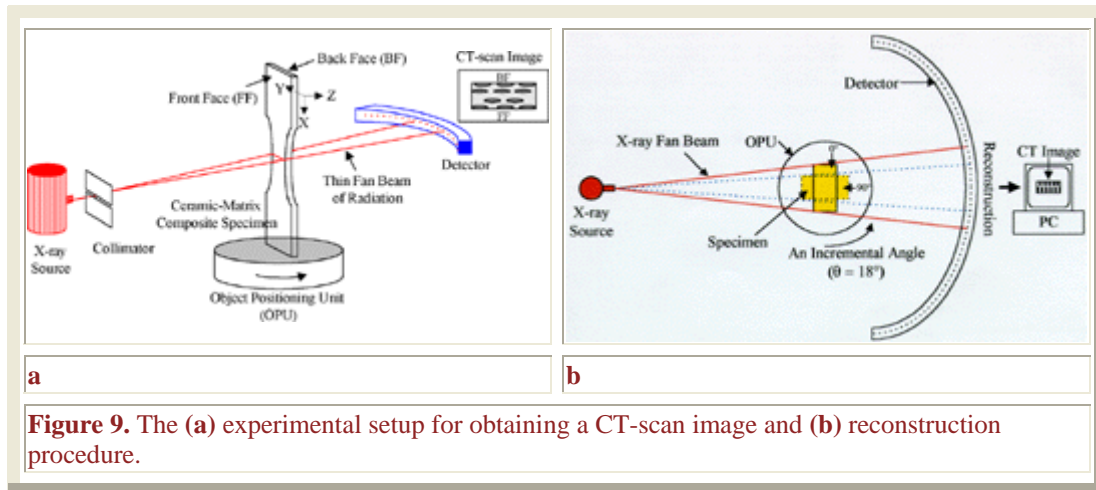


Figure 9 illustrates the CT setup and reconstruction procedure. As shown in Figure 9a, a CT system typically contains a tungsten x-ray radiation source and a cadmium/tungstate radiation detector as well as a precision manipulator to scan cross-sectional slices from different angles. The x-ray source, which can be operated at 420 kV and 3 mA, is collimated to form a thin fan beam. The fraction of the attenuated x-ray beam is directly related to the density and thickness of the test object, the composition of the material, and the energy of the x-ray beam. To obtain a full set of imaging data, the test subject, x-ray source, or detector array moves and a sequence of measurements is made from multiple incremental angles ( $\theta$ ). The data-acquisition system reads the signal from each detector in the array, converts the measurements into numeric values, and transfers the data to a computer for digital reconstruction. The

reconstruction process (Figure 9b) uses an algorithm to identify the point-by-point distribution of the x-ray densities in the two-dimensional image of the cross-sectional slice.<sup>23</sup> In the example depicted in Figure 9b, the incremental rotation angle equals 18°; this means that ten different cross-sectional views were collected in order to construct a CT image.

The fundamentals of CT are described in the sidebar.

## CT THEORY

Since CT images are related to x-ray radiation, attenuation is followed by Lambert's law of absorption. In the simplest case, the linear absorption coefficient can be expressed by<sup>23</sup>

$$I = I_0 e^{-\mu x} \quad (A)$$

where  $I$  is the intensity of the transmitted x-ray beam after passing through thickness  $x$ ,  $I_0$  is the intensity of the incident beam, and  $\mu$  is the linear absorption coefficient. When x-rays penetrate a nonhomogeneous material, the general expression for absorption should be

$$I = I_0 e^{-\int \mu(s) ds} \quad (B)$$

where,  $\mu(s)$  is the linear absorption coefficient at each point on the x-ray path. Rearranging Equation B yields

$$-\ln(I/I_0) = \int \mu(s) ds \quad (C)$$

The CT reconstruction procedure includes two basic types of transform methods: the convolution-backprojection algorithm and the direct Fourier algorithm. Fundamental concepts of these methods are such that the one-dimensional Fourier transform of a CT projection for an object corresponds to a spoke in the Fourier space of the two-dimensional transform of that object. After transforming each collected projection, it is necessary to invert the two-dimensional Fourier transform to obtain the final image (the direct Fourier transform algorithm). Through the convolution-backprojection methods, the results of Equation C can be rearranged in the following form:

$$P(\theta, \rho) = -\ln[I(\theta, \rho)/I_0] = \int \mu(x, y) ds \quad (D)$$

where  $I$  is a single ideal measurement of the intensity (representing the oriented detector with respect to the object with the incremental angle,  $\theta$ , and position,  $\rho$ ),  $\mu(x, y)$  is a two-dimensional distribution of the linear attenuation coefficient for the object, and  $ds$  is an element of the distance along the x-ray path through the object at an angle,  $\theta$ , and position,  $\rho$ . The values of  $I(\theta, \rho)$  are normalized to unity and logged to yield a set of estimated line integrals through the object,  $P(\theta, \rho)$ . Thus, the convolution-backprojection process can be written as follows:

$$\mu(x, y) = \int_0^\pi \int_{-\infty}^{\infty} P(\theta, \rho) g(\rho - r) d\rho d\theta \quad (E)$$

where  $g$  is the convolution (filter) function of the shape-theoretical form and

$$g(r) = \frac{\pi^2}{2} \left( \frac{\delta(r)}{r} - \frac{1}{r^2} \right) \quad (F)$$

where  $\delta(r)$  is the Dirac delta function, and  $r$  is the radius of a reconstruction circle.

From Equations E and F,  $\mu(x, y)$  can be recovered from a complete set of line integrals,  $P(\theta, \rho)$ , by first

convolving each projection with a special function,  $g$  (i.e., the integral over  $\eta$  in Equation E), and backprojecting each convolved view to obtain a final image (i.e., the integral over  $\theta$  in Equation E).

Convolving the views with the function,  $g$ , given in Equation F serves two purposes:

1. A polar-coordinate version of the delta function that serves to preserve the basic profile of each view.
2. Correction for the blurring introduced by the backprojection algorithm.

Note that if the convolution is conducted in a direct space (i.e., the inner integral in Equation E is evaluated directly), the method is called convolution-backprojection; if it is conducted in a Fourier space (which is generally a much faster approach), the technique is called filtered-backprojection. This distinction is frequently overlooked, and the two terms are often used interchangeably. In our research, the filtered-backprojection technique is used to investigate ceramic-matrix composites.

## Experimental Activities

CT was used to demonstrate the correlation between the transmitted ultrasonic amplitude of a C-scan and the extent of porosity and/or internal flaws. Figure 10 shows C-scans and CT scans for plain-weave Nicalon/SiC and cross-ply Nicalon/SiC composites (CT scans were taken along the specimen width). The defects seem to be distributed through the whole specimen.

The CT scans were made through three different cross sections for each specimen, as indicated by the letters A, B, and C (the adjoining numbers identify the samples). These sections were carefully chosen to relate the ultrasonic C-scan images with the CT results. For example, the sections of the woven composite were chosen as the best (A), worst (B), and intermediate (C) C-scan amplitude distributions. Note that A and C are located in the grip sections of the samples, while B is from the gage section.

A visual examination of the C-scan versus the CT images shows a reasonably good relationship between the amount of porosity and the transmitted amplitudes. The dark areas in the CT images indicate the presence of porosity and/or defects in the composites. In the case of the woven specimen (Figure 10a), 3A includes fewer defects and, correspondingly, greater ultrasonic wave amplitudes than any other section. The CT results present a good correlation with the C-scan data. Specifically, the CT-scan of 3A shows less porosity than sections 3B or 3C.

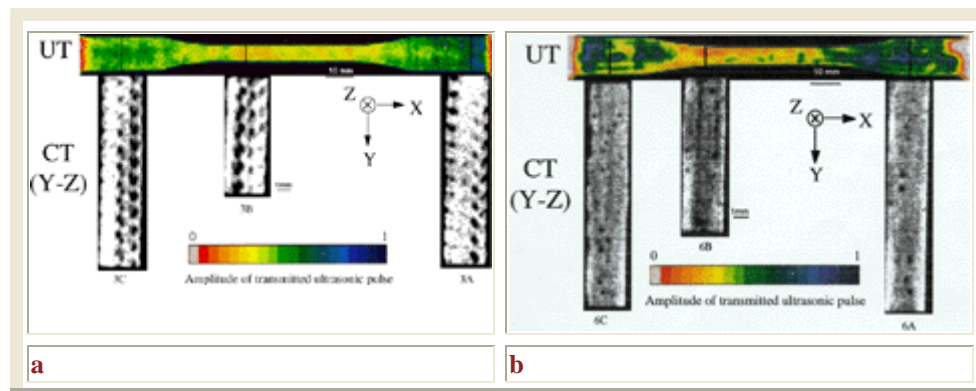


**Figure 10.** Ultrasonic C-scans and CT scans for (a) woven (sample 3) and (b) 0°/90° cross-ply (sample 6) Nicalon-fiber-reinforced composites. Note that the CT-scans are along the width direction (Y-Z plane) of the sample.

To quantify the CT results, a porosity calculation was performed. The regions containing porosity and/or defects are black on the CT scans; the white regions are regarded as defect-free. A relative color distinction between the white and black regions is made possible by calculating the amount of porosity and/or defects in the CT results.

In analyzing the relationship between the ultrasonically transmitted amplitudes and the volume of porosity along the width of the woven and cross-ply composite specimens, it was observed that, in both cases, the ultrasonically transmitted amplitude decreases as porosity increases. Indeed, there is an exponential relationship between the ultrasonically transmitted amplitude and the amount of porosity, which provides an effective and consistent way to assess the quality of continuous-Nicalon-fiber-reinforced silicon carbide composites using both UT and CT.

The exponential function of this relationship is derived according to the following equation:<sup>13</sup>

$$\frac{A}{A_0} = \exp(-nrf) \quad (2)$$

where the ratio  $A/A_0$  is the relative ultrasonic transmitted amplitude,  $n$  is the number density for porosity, and  $f$  is a constant.

Recently, CT has been extensively used to characterize ceramic components, including ceramic failure analysis,<sup>24</sup> composite-structure developments,<sup>25</sup> and microstructural characterization in ceramic composites.<sup>26</sup>

## ACOUSTIC EMISSIONS

AE can be a very powerful NDE technique for the in-situ monitoring of damage evolution during mechanical testing. When a material is subjected to stress, it experiences plastic deformation, the formation of flaws, or fracture; these conditions produce small stresses or ultrasonic waves in the material and acoustic emissions are generated. For ceramic materials, an increase in acoustic emissions occurs before fracture, providing a potential means of either detecting crack initiation or predicting when failure is imminent. Acoustic emissions can be detected by AE piezoelectric sensors (transducers), which convert wave pulses into electrical impulses that can be amplified and displayed.<sup>3,6</sup>

The process of wave generation and detection is shown in Figure 11a.<sup>27</sup> Generally, AE equipment includes piezoelectric transducers, amplifiers, single- and multi-channel signal processing systems, acoustic-event counters, and coordinate plotters.<sup>3,5</sup> A typical AE signal is shown in Figure 11b along with such AE parameters as amplitude (the highest peak voltage attained by an AE waveform), counts (the threshold-crossing pulses), energy counts (the measured area under the rectified signal envelope), duration (the elapsed time from the first threshold crossing to the last), and rise time (the elapsed time from the first threshold crossing to the signal peak).<sup>27</sup>

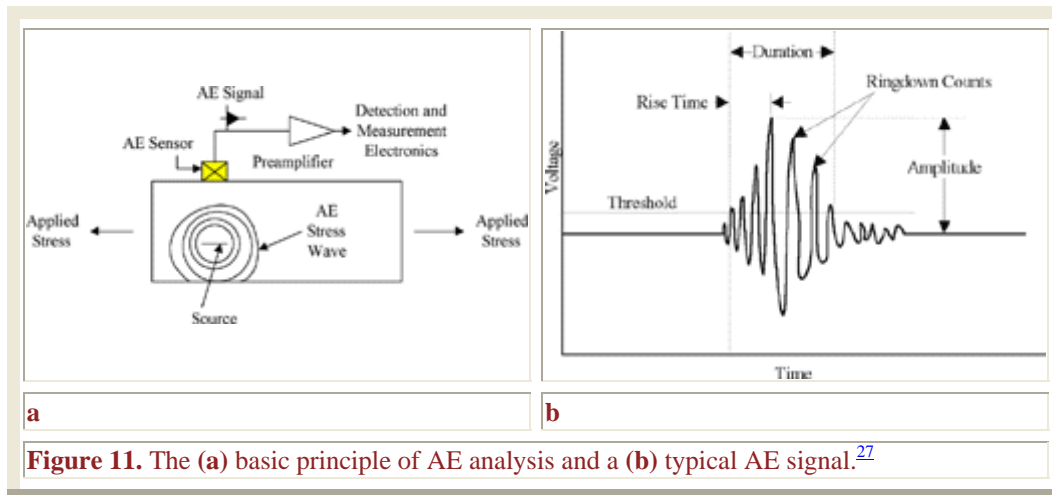


**Figure 11.** The (a) basic principle of AE analysis and a (b) typical AE signal.<sup>27</sup>

Generally, the AE output can be in either continuous or burst forms. A continuous emission means the signal amplitudes are slightly higher than the background noise; the AE events are closely spaced in terms of time and form a single waveform. A burst emission occurs when the signal amplitudes are larger than the background noise; the AE events are of a short duration and are well separated in terms of time. Usually, a cracking event can be detected by a short rise time and exponential decay.<sup>28</sup>

In terms of ceramic-based materials, the rate and intensity of acoustic emissions may be used to detect the initiation and propagation of cracks and delaminations,<sup>29-32</sup> and acoustic emission NDE can be used to predict static and fatigue failure.<sup>33</sup>

## Experimental Activities

AE was used to investigate stress-strain behavior and observe damage mechanisms in ceramic-matrix composites during tensile testing.<sup>29-32</sup> The measurements were correlated with macroscopic stress-strain behavior and direct microscopic observation of damage development in unidirectional Nicalon/CAS composites. AE events represent matrix cracking above the proportional limit of the stress-strain curve under monotonic tensile loading. In the case of loading-unloading cycles, fiber-matrix debonding and fiber pull-out procedures were successfully monitored based on changes in the AE rate and cumulative AE counts.

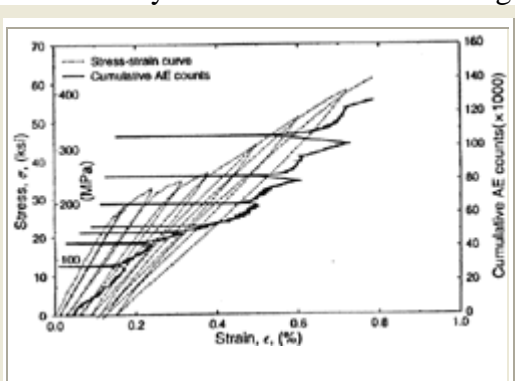


**Figure 12.** Stress and cumulative AE counts versus strain for the loading and unloading a unidirectional SiC/CAS composite under longitudinal tension.<sup>30</sup>

Figure 12 presents a representative stress-strain curve versus AE counts for loading and unloading.<sup>30</sup> The locus of the cumulative AE counts shows the classical Kaiser effect—emissions derived from repeated loading sequences indicate that structural damage occurred between the first loading and the reapplication of the load; there are no emissions until the previous load level is reached again.<sup>27</sup> Similar work has been performed on different lay-ups, such as unidirectional, cross-ply, quasi-isotropic, angle-ply, and continuous Tyranno SiC fiber-reinforced barium-magnesium aluminosilicate (SiC/BMAS) composites during displacement-controlled tensile testing.<sup>29</sup> (The typical fiber composition, in weight percent, was

44% Si, 25% C, 12% O<sub>2</sub>, 3% N<sub>2</sub>, and 11% Ti.) Both the cumulative number of AE events (to detect damage initiation and evolution) and AE characteristics, such as event duration and energy (to discriminate between damage modes), were used to monitor damage development in the SiC/BMAS composites.

Shiwa et al. investigated fracture mechanisms in SiC/SiC composites using AE analysis.<sup>31</sup> Monitored during tensile testing were such fracture mechanisms as matrix cracking, crack deflection, interface debonding, and fiber pull-out. The AE amplitude distribution was used to determine the corresponding fracture mechanisms.

AE analysis also has been used to predict fatigue failure in ceramic materials subjected to cyclic mechanical loading.<sup>33</sup> It was capable of predicting failure by showing an increase in the energy/count rate prior to failure during tension-tension fatigue loading.

## CONCLUSIONS

Among the NDE techniques described in this paper, the best approach is always the method that yields the most efficient results for a given application. When possible, a combination of techniques can be used to the greatest benefit.

The main advantages of UT are the ability to investigate relatively thick materials and obtain test results quickly. The approach does, however, require an acoustic coupling media. CT provides a cross-sectional view of the entire material, but the equipment cost is expensive. The technique, along with radiography, also raises issues of radiation safety. AE is a unique method in that it provides continuous surveillance during the testing, but it requires a prehistory of stresses for defect detection.

## ACKNOWLEDGEMENTS

*This work is supported by the [National Science Foundation](#), under contracts EEC-9527527 (with Mary Poats as a contract monitor) and DMI-9724476 (with Delcie Durham as monitor). The authors are grateful to D.K. Hsu, W.A. Simpson, Jr., and D.J. McGuire for our current research efforts and their most kind help on UT and CT.*

## References

1. R.L. Lehman, S.K. El-Rahaiby, and J.B. Wachtman, *Handbook on Continuous Fiber-Reinforced Ceramic Matrix Composites* (New York: [ACerS](#), 1995), p. 495.
2. L. Cartz, *Nondestructive Testing* (Materials Park, OH: [ASM](#), 1995).
3. M.M. Schwartz, *Composite Materials*, vol. 1 (Upper Saddle River, NJ: [Prentice-Hall](#), 1997).
4. D.E. Bray and D. McBride, *Nondestructive Testing Techniques* (New York: [John Wiley & Sons](#), 1992).
5. P.E. Mix, *Introduction to Nondestructive Testing* (New York: [John Wiley & Sons](#), 1987).
6. D.W. Richerson, *Modern Ceramic Engineering*, 2nd ed. (New York: [Marcel Dekker](#), 1992).
7. *Standard Terminology for Nondestructive Examinations*, E1316-96 (Philadelphia, PA: [ASTM](#), 1996).
8. P. Holler et al., eds., *Nondestructive Characterization of Materials* (1988).

9. [ASM Handbook: Nondestructive Evaluation and Quality Control](#), vol. 17 (Materials Park, OH: [ASM](#), 1992), p. 231.
10. A. Kelly: *Concise Encyclopedia of Composite Materials* (New York: [Pergamon](#), 1989), p. 199.
11. J. Kim et al., "Nondestructive Evaluation of Continuous Nicalon Fiber Reinforced Silicon Carbide Composites," [Nondestructive Evaluation and Materials Properties III](#), ed. P.K. Liaw et al. (Warrendale, PA: [TMS](#), 1997), pp. 55-63.
12. J. Kim et al., "Nondestructive Evaluation of Nicalon/SiC Composites by Ultrasonics and X-ray Computed Tomography," *Ceramic Engineering and Science Proceedings*, 18 (4) (1997), pp. 287-296.
13. P.K. Liaw et al., "Nondestructive Evaluation of Woven Fabric Reinforced Ceramic Composites," *Nondestructive Evaluation of Ceramics*, *Ceramic Transactions*, vol. 89, ed. C. Schilling et al. (1998), pp. 121-135.
14. P.K. Liaw et al., *Acta Metall.*, 44 (5) (1996), p. 2101.
15. [ASNT Handbook: Nondestructive Testing Handbook](#), 2nd ed., vol. 3 (Columbus, OH: [ASNT](#), 1985).
16. Y. Nir-El et al., *Nondestructive Testing and Evaluation*, 11 (1994), pp. 149-153.
17. W.J. Lewis et al., *Nondestructive Testing and Evaluation*, 11 (1994), pp. 155-164.
18. S. Ekinici and A.N. Bilge, *British Journal of NDT*, 33 (9) (1991), pp. 450-452.
19. P.C. Copley, J.W. Eberhand, and G.A. Mohr, *JOM*, 46 (1) (1994), pp. 14-26.
20. [ASM Handbook: Nondestructive Evaluation and Quality Control](#), vol. 17 (Materials Park, OH: [ASM](#), 1992), p. 358.
21. J.C. Elliott et al., *JOM*, 46 (3) (1994), p. 11.
22. S.R. Stock et al., *JOM*, 47 (1) (1995), p. 19.
23. [Standard Guide for Computed Tomography Imaging](#), E1441-95 (Philadelphia, PA: [ASTM](#), 1995).
24. R.H. Bossi, D.A. Cross, and R.A. Mickelsen, *Proceedings of the 22nd International Symposium for Testing and Failure Analysis* (1996), pp. 77-82.
25. R.H. Bossi and G.E. Georgeson, *Materials Evaluation*, 53 (October 1995), pp. 1198-1203.
26. B. London, R.N. Yancey, and J.A. Smith, *Materials Evaluation*, 48 (May 1990), pp. 604-608.
27. [ASM Handbook: Nondestructive Evaluation and Quality Control](#), vol. 17 (Materials Park, OH: [ASM](#), 1992), p. 284.
28. C. Lin et al., *J. Am. Ceram. Soc.*, 80 (9) (1997), pp. 2382-2394.
29. M. Surgeon et al., *Composites*, 28A (1997), pp. 473-480.
30. J. Luo, S. Wooh, and I.M. Daniel, *J. Comp. Mat.*, 29 (15) (1995), pp. 1946-1961.
31. M. Shiwa et al., *Materials Transactions, JIM*, 36 (4) (1995), pp. 511-517.
32. G.N. Morscher, to be published in *Composite Science and Technology*.
33. O.M. Jadaan, K.C. Liu, and H. Pih, *Proceedings of the 10th ASME Design Technical Conference*, vol. 55 (Fairfield, NJ: [ASME](#), 1993), pp. 93-104.

## ABOUT THE AUTHORS

**Jeongguk Kim** earned his B.E. in inorganic materials engineering at [Pusan National University](#) in 1987. He is currently a Ph.D. student at the [University of Tennessee at Knoxville](#). Mr. Kim is also a member of [TMS](#).

**Peter K. Liaw** earned his Ph.D. in materials science and engineering at [Northwestern University](#) in 1980. He is currently professor and Ivan Racheff Chair of Excellence in the

[Department of Materials Science and Engineering](#) at the [University of Tennessee at Knoxville](#). Dr. Liaw is also a member of [TMS](#).